Monolayers and 3D Films of Cholesteryl Derivatives at the Air−Water Interface

P. Viswanath and K. A. Suresh*

Raman Research Institute, Sadashivanagar, Bangalore 560 080, India

Received: February 6, 2004; In Final Form: April 20, 2004

Cholesterol and its derivatives have drawn much attention because of their relevance to biology. They have also been studied at the air−water (A−W) interface. Here, we have systematically investigated the two-dimensional (2D) and three-dimensional (3D) phases of cholesteryl derivatives at the A−W interface employing surface manometry, epifluorescence, Brewster-angle and reflection microscopy techniques. We found that the short-chain ester cholesteryl acetate forms a stable monolayer. The higher homologues cholesteryl heptanoate and cholesteryl octanoate do not form monolayers; they yield 3D crystallites at very large area per molecule. Interestingly, we found cholesteryl nonanoate to be in the crossover regime in the homologous series of cholesteryl esters. It spontaneously forms a fluidlike bilayer at the A−W interface. The higher homologue cholesteryl laurate forms an unstable bilayer phase. The long-chain esters cholesteryl myristate, cholesteryl palmitate, and cholesteryl stearate exhibit crystalline bilayer and 3D structures. Cholesteryl benzoate, which contains a bulkier phenyl group instead of the flexible alkyl chain, forms a crystalline bilayer. We discuss the assembly of molecules in the different phases at the A−W interface for the cholesteryl derivatives with respect to their packing in the bulk and the onset of the smectic liquid-crystalline phase.

1. Introduction

Cholesteryl esters are found in the interior lipid core of chylomicrons and in lipoproteins.[1] Cholesteryl esters are also found in atherosclerotic lesions.[2] The higher homologues of cholesteryl ester take part in hydrolysis and are responsible for the transport of free cholesterol.[3] Some cholesteryl esters also exhibit liquid-crystalline phases. Thus, a study of the assembly of the molecules of cholesteryl esters at the air−water (A−W) interface is of considerable interest and has drawn much attention. Langmuir films of sterol and short-chain cholesteryl esters have been studied with an emphasis on the nucleation and crystallization process at the A−W interface[4] and on the inhibition of crystallization of these sterols in lipids.[5] Short-chain derivatives of cholesteryl esters such as formate and acetate have been reported to form stable monolayers.[6,7] The higher homologues of cholesteryl ester, such as cholesteryl myristate, cholesteryl palmitate, and cholesteryl stearate were shown to form unstable monolayers at the A−W interface.[7] In the cases of cholesteryl palmitate and cholesteryl stearate, recent studies have suggested the coexistence of a bilayer with thicker domains.[8] However, for some other intermediate homologues of cholesteryl derivatives, no studies have been performed on the monolayer properties at the A−W interface. Techniques such as epifluorescence[9,10] and Brewster-angle microscopy[11] are valuable tools for probing monolayers as well as 3D films at the A−W interface. In the literature, it appears that there are not many reports on cholesteryl derivatives employing these techniques.

In this paper, we describe our investigations on the phases, aggregation, and structure of films of cholesteryl derivatives at the A−W interface. On the basis of our surface manometry and microscopy studies, we found that the short-chain esters of cholesterol, such as cholesteryl acetate, form stable monolayers. Cholesteryl heptanoate and cholesteryl octanoate do not form monolayers; rather, they yield irreproducible isotherms and form three-dimensional (3D) crystallites at the A−W interface. Interesting behavior was seen for the next homologue, cholesteryl nonanoate. Here, a spontaneously formed bilayer was seen to coexist with the gas phase at the A−W interface. The higher homologue cholesteryl laurate exhibits a bilayer phase with a tendency to crystallize during compression even at very low surface pressures. Still higher homologues such as cholesteryl myristate, cholesteryl palmitate, and cholesteryl stearate form crystalline bilayers and coexist with 3D structures (i.e., multilayers coexisting with crystallites). We found that cholesteryl benzoate forms a crystalline bilayer phase even at large area per molecule. We compare the packing of the molecules in the different phases at the A−W interface for some of the cholesteryl derivatives with their packing in the bulk as reported from X-ray diffraction studies.[12]

2. Experimental Section

In our studies, we have used the following materials: (1) cholesterol (Ch), (2) cholesteryl acetate (ChA), (3) cholesteryl heptanoate (ChH), (4) cholesteryl octanoate (ChO), (5) cholesteryl nonanoate (ChN), (6) cholesteryl laurate (ChL), (7) cholesteryl myristate (ChM), (8) cholesteryl palmitate (ChP), (9) cholesteryl stearate (ChS), (10) cholesteryl benzoate (ChB), (11) cholesteryl hydro cinnamate (ChHC), (12) cholesteryl oleate (ChOl), and (13) cholesteryl oleyl carbonate (ChOC). These were obtained from Sigma and Aldrich. The materials Ch, ChA, ChH, ChO, ChN, ChL, ChM, ChS, ChP, ChB, and ChHC were recrystallized twice, and their purities were checked by thin-layer chromatography. Their melting points were checked using a Mettler hot stage. The materials ChOl and ChOC were used as received. The surface manometry experiments were carried out using a Nima 611M trough. The subphase used was Millipore Milli-Q water with a pH of 5.7. The relative humidity was maintained around 85 ± 5%. A solution of concentration 1 mg/mL was prepared using chloroform (HPLC grade) as the

* Corresponding author. E-mail: suresh@rri.res.in.

10.1021/jp049454z CCC: $27.50
Published on Web 05/29/2004

solvent. Small drops of solution were spread all over the trough between the barriers using a microsyringe (Hamilton). The system was left for 10 min to allow the solvent to evaporate. The entire trough was enclosed inside a Perspex box to prevent contamination and air drag and to minimize water evaporation. The surface pressure was measured using the standard Wilhelmy plate technique with filter paper. The monolayers were compressed at a speed of 4 cm^2/min. This corresponds to a compression rate in the range of 0.5−1 ($Å^2$/molecule)/min for the materials from Ch to ChS. All of the experiments were carried out at a temperature (t) of 25 ± 1 °C.

The equilibrium spreading pressure (ESP) for cholesteryl derivatives was measured at a constant area of 100 cm^2. High humidity of the order of 92 ± 5% was maintained during the experiments to prevent any evaporation. To determine the ESP value, we monitored the surface pressure with time. Epifluorescence microscopy was employed to characterize the phases indicated by the surface pressure (π) vs area per molecule (A/M) isotherm studies. A fluorescent dye, namely, 4-(hexadecylamino)-7-nitrobenz-2 oxa-1,3 diazole (Molecular Probes), of about 1% molar concentration was added as a dopant to the solution. The monolayer was observed under a Leitz Metallux 3 microscope. The light source was a high-pressure mercury lamp (100 W). Appropriate wavelength suitable for the fluorescent dye was chosen using dichroic filters. The images were obtained using a photon-intensified CCD camera (model P 46036A/V22, EEV). A Brewster-angle microscope (BAM) was also employed to observe the films of cholesteryl derivatives at the A−W interface. The advantage of this technique over epifluorescence microscopy is that it does not require a fluorescent dye. However, the resolution in our epifluorescence microscope images is much better than that in the BAM images. We used a MiniBAM (NFT, Nanotech) in the experiments. Here, a p-polarized laser beam of wavelength of 660 nm and a power of 30 mW was incident on the A−W interface at the Brewster angle. The reflected light from the film at the A−W interface was sensed by a detector. The BAM technique in combination with epifluorescence microscopy provided textures with different spatial length scales. Thicker films can be studied using microscopy techniques such as light scattering[13] and reflection.[14] In reflection microscopy, a Leitz Metallux 3 microscope incorporated with a half-silvered mirror was used. This allows the white light from the mercury lamp to be incident normally on the film at the A−W interface. The light beam gets reflected from the film−air and subphase−film interfaces, leading to interference patterns. In this modified setup, the half-silvered mirror or the dichroic filters can be flipped alternately to view the film in reflection or epifluorescence mode, respectively. The images were recorded using a Sony CCD (DXC-390P) camera.

3. Results

Surface pressure (π)−area per molecule (A/M) isotherms of cholesteryl derivatives are shown in Figure 1. For cholesterol, a limiting area per molecule (A_0) value of 38.8 $Å^2$ and a collapse pressure (π_c) of 43 mN/m were obtained from the $\pi-A/M$ isotherm. These values are in good agreement with the reported values.[5,15] Cholesteryl acetate exhibited an isotherm similar to that of Ch, yielding a collapse pressure of 16.0 mN/m and an A_0 value close to that of Ch. The esters cholesteryl heptanoate and cholesteryl octanoate did not form stable monolayers at the A−W interface. The $\pi-A/M$ isotherm for cholesteryl nonanoate is shown in the inset of Figure 1. Compression of the ChN film led to a rise in the surface pressure around 22.5 $Å^2$. This was

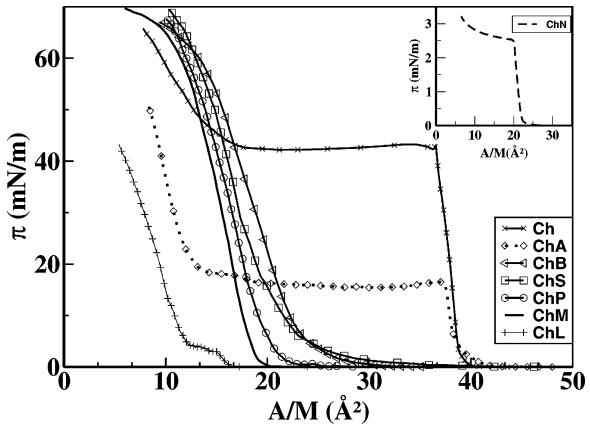

Figure 1. Surface pressure (π)−area per molecule (A/M) isotherms of cholesteryl derivatives at a temperature of $t = 25$ °C. The isotherms are shown for cholesterol (Ch), cholesteryl acetate (ChA), cholesteryl benzoate (ChB), cholesteryl stearate (ChS), cholesteryl palmitate (ChP), cholesteryl myristate (ChM), and cholesteryl laurate (ChL). The inset shows the $\pi-A/M$ isotherm for cholesteryl nonanoate (ChN).

followed by a collapse at a surface pressure of 2.5 mN/m with an A_0 value of 22 $Å^2$. After the collapse, there was a marginal increase in the surface pressure. The isotherm for cholesteryl laurate is shown in Figure 1. Upon compression, there was an increase in the surface pressure around 17.3 $Å^2$, and the film collapsed at a surface pressure of 3.0 mN/m. The isotherm yielded an A_0 value of 16.3 $Å^2$. After the collapse, there was a gradual increase in the surface pressure up to about 4.4 mN/m. From then onward, the surface pressure increased rapidly to a value of about 45 mN/m at an A/M value of about 5 $Å^2$. Cholesteryl myristate, cholesteryl palmitate, and cholesteryl stearate have longer alkyl chains. Cholesteryl benzoate contains a bulkier phenyl ring, which is different from the flexible alkyl chains of cholesteryl esters. Interestingly, these four molecules exhibited similar behaviors in the $\pi-A/M$ isotherms that were different from the behaviors of other cholesteryl derivatives. For ChM molecules, microcrystallites could be directly seen at the A−W interface immediately after spreading at a concentration of 1 mg/mL. At large A/M, the surface pressure of ChM exhibited fluctuations during compression. The ChM film, at surface pressures corresponding to the steep region of the isotherm, appeared quite rigid at the A−W interface. The isotherm yields an A_0 value of 19.6 $Å^2$, indicating bilayer formation when compared to its estimated cross-sectional area. The isotherms for ChP and ChS yielded A_0 values of 20.7 and 21.4 $Å^2$, respectively, again indicating bilayer formation. The isotherm for ChB shows a slightly higher A_0 value of 23.7 $Å^2$, which, compared to its cross-sectional area of about 48 $Å^2$, indicates a bilayer. The collapse pressures of ChM, ChP, ChS, and ChB were nearly the same at about 60 mN/m. The $\pi-A/M$ isotherms of cholesteryl oleate and cholesteryl oleyl carbonate yielded A_0 values of 114.3 and 28.7 $Å^2$, respectively (see Supporting Information).

The equilibrium spreading pressure (ESP) is the surface pressure at which a monolayer coexists with its bulk phase. The ESPs of Ch and ChA were around 38.1 and 7.1 mN/m, respectively. For Ch, the ESP was attained within a period of 10 min. For ChA, the time scale for the molecules to elute from the crystallites was very slow and was of the order of a few hours.

Our epifluorescence microscopy images for Ch monolayer were very similar to those reported by Slotte and Mattjus.[15] Hence, we have not presented the images. Under the epifluorescence microscope, we found the coexistence of gas (G) and

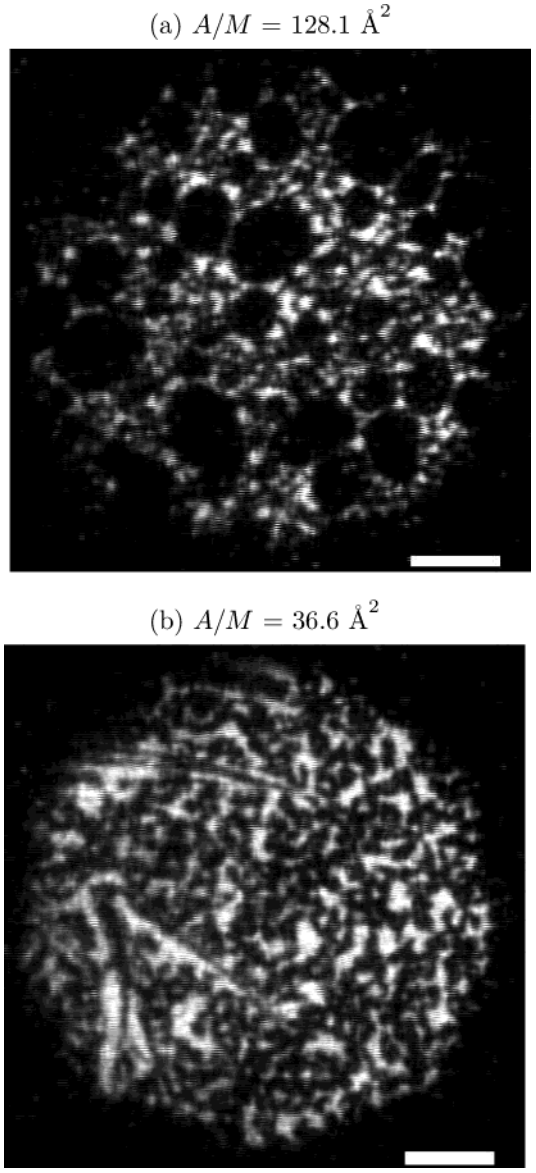

Figure 2. Epifluorescence images of cholesteryl acetate. (a) Coexistence of gas (dark) domains with the L_2 phase. The L_2 phase appears as a meshlike texture. (b) Collapsed state. Here, the ChA crystallites (dark streaks) coexist with the L_2 phase (mesh texture). The scale bar represents 50 μm.

L_2 phases[16] that, on compression, transformed into a homogeneous L_2 phase. Further compression led to a collapsed state in which we found the coexistence of the L_2 phase and 3D crystallites. In the case of ChA, the textures were very different from those of Ch. Epifluorescence images of ChA are shown in Figure 2. At very large *A*/*M*, we could observe the usual circular G domains coexisting with the L_2 phase. Upon compression, the G domains diminished in size (Figure 2a) and gave rise to the L_2 phase, which exhibited a meshlike texture. These L_2 domains exhibited irregular boundary and were less mobile. These observations indicated the crystalline nature of the L_2 monolayer phase. In the collapsed state, 3D crystallites (dark streaks) of ChA were seen to coexist with the L_2 phase (Figure 2b). For ChH and ChO, there were no indication of the usual G and L_2 monolayer phases; these materials formed only 3D crystallites.

The epifluorescence microscope images of ChN revealed interesting features, as shown in Figure 3. Figure 3a shows the coexisting G (dark) and condensed (gray domains) phases. This

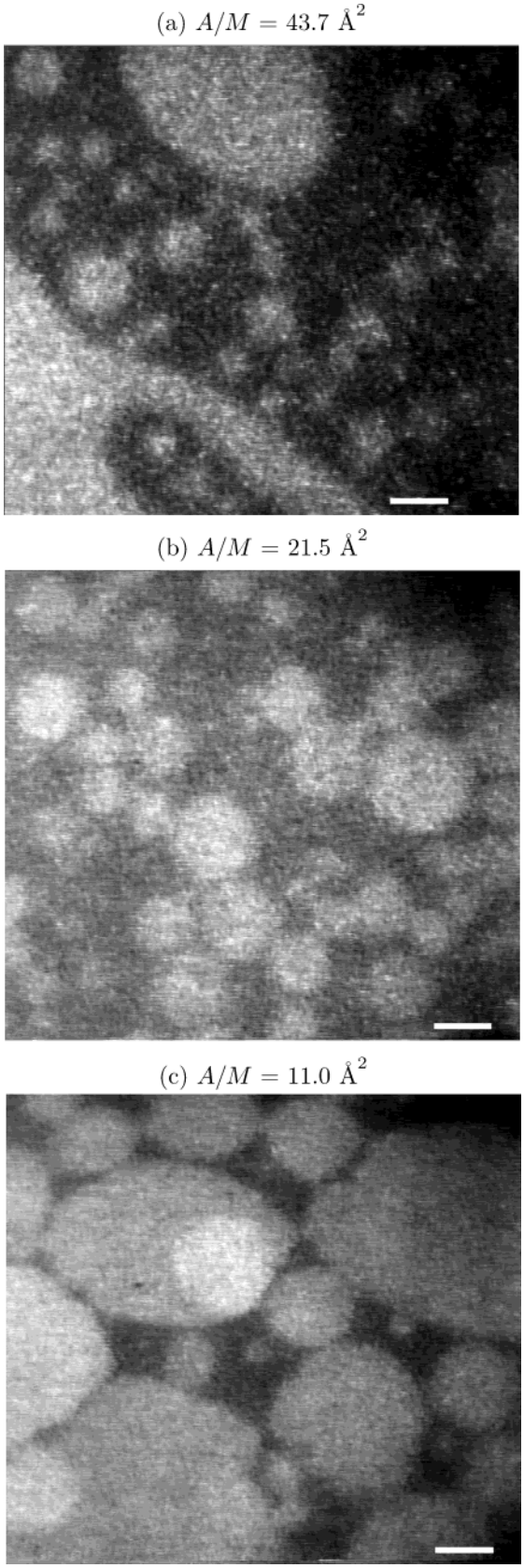

Figure 3. Cholesteryl nonanoate images under the epifluorescence microscope. (a) Coexistence of gas (dark) and condensed (gray) phases. (b) Collapsed state. Here, the bright circular 3D domains are seen to coexist with a background condensed (gray) phase. (c) Collapsed state at very low *A*/*M*. Here, the 3D domains were in a metastable state and transformed from a circular shape to distorted structures. Inside these 3D domains, still brighter domains were seen to nucleate. The scale bar represents 50 μm.

(a) $A/M = 45.8$ Å^2

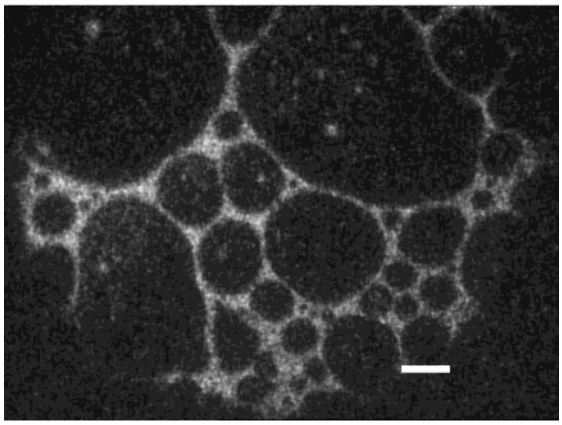

(b) $A/M = 40.4$ Å^2

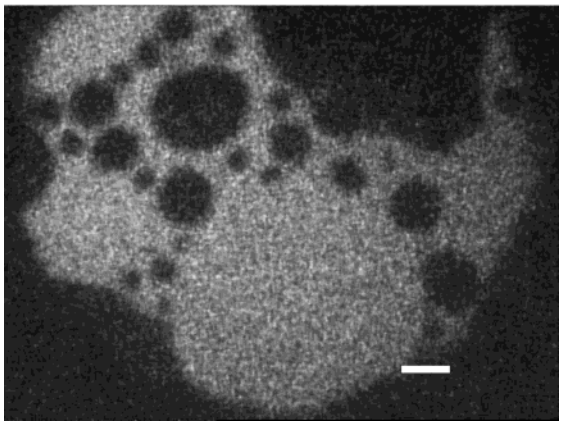

Figure 4. Cholesteryl laurate images under the epifluorescence microscope seen at very low surface pressure (~0.1 mN/m). (a) Coexistence of gas (dark) and condensed (gray) phases. The condensed phase was more mobile. (b) Coexistence of the condensed phase, bright circular 3D domains, and the gas phase in the background. The scale bar represents 50 μm.

(a) $A/M = 81.8$ Å^2

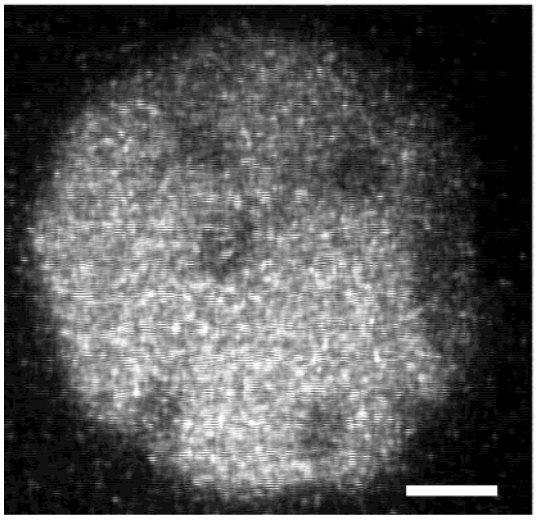

(b) $A/M = 28.0$ Å^2

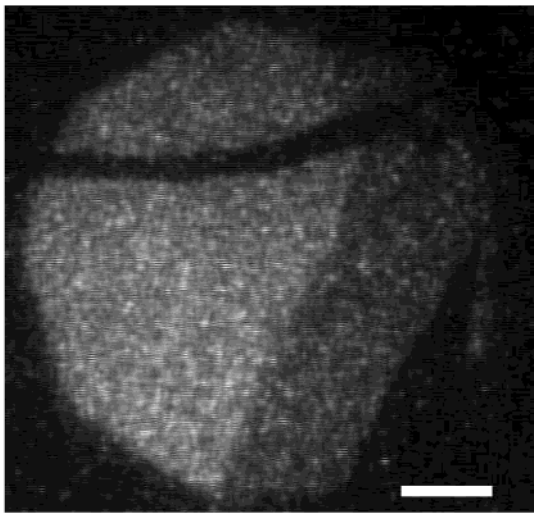

Figure 5. Cholesteryl myristate images under the epifluorescence microscope seen at very low surface pressure (~0.1 mN/m). (a) Presence of dark regions over the 3D structures. (b) Presence of 3D structures with varying intensity, revealing the variation in thickness. The scale bar represents 50 μm.

was followed by a transition to an uniform condensed phase. The condensed phase was more mobile. In the collapsed state, bright circular 3D domains (a pattern exhibiting uniform intensity and having a smooth periphery) were seen to coexist with the condensed phase (Figure 3b). Upon further compression, the 3D domains grew in size and became distorted from the circular shape (Figure 3c). At this stage, we could see the nucleation and growth of still brighter domains. Epifluorescence images for ChL are shown in Figure 4. At large *A*/*M*, coexisting G (dark) and condensed (gray regions) phases were seen (Figure 4a). They exhibited a foamlike texture. The condensed phase was quite mobile. Upon compression, bright circular 3D domains of varying intensities were seen to nucleate from the condensed phase (gray) and coexist with the G phase (Figure 4b). Upon further compression, these bright 3D domains became distorted from their circular shape and grew at the expense of the condensed phase. These textural changes were observed even at zero surface pressure. Epifluorescence images for ChM are shown in Figure 5. For ChM, we found 3D structures with fractured edges and voids (gas phase) even at very large *A*/*M* (see Supporting Information). At lower *A*/*M*, dark patches were seen on these 3D structures (Figure 5a). At still lower *A*/*M*, the epifluorescence images showed structures of varying intensity, which indicated 3D structures of different thicknesses (Figure 5b). The textures of ChP were similar to those of ChM under the epifluorescence microscope at large *A*/*M*. The epifluorescence images for ChS are shown in Figure 6. The textures showed circular as well as distorted 3D crystalline structures with varying intensities coexisting with the G phase (Figure 6a). Further compression led to the disappearance of voids. In the collapsed state, formation of bright streaks were seen over these 3D structures (Figure 6b). Our epifluorescence studies for ChB show the coexistence of gas (dark) and crystalline gray domains. The dispersion of the fluorescent dye was not good in this system. Further compression predominantly led to a crystalline phase. The film was less mobile, indicating high crystallinity. Cholesteryl hydro cinnamate images showed the formation of 3D crystallites even at very large *A*/*M* of the order of 300 Å^2.

Brewster-angle microscopy was employed to check the different phases seen by epifluorescence microscopy. Our BAM images of Ch were very similar to those reported by Seoane et al.[17] Hence, we have not presented the BAM images here. We found coexisting G and L_2 phases. With compression, the structure transformed to L_2 phase. After the collapse, bright

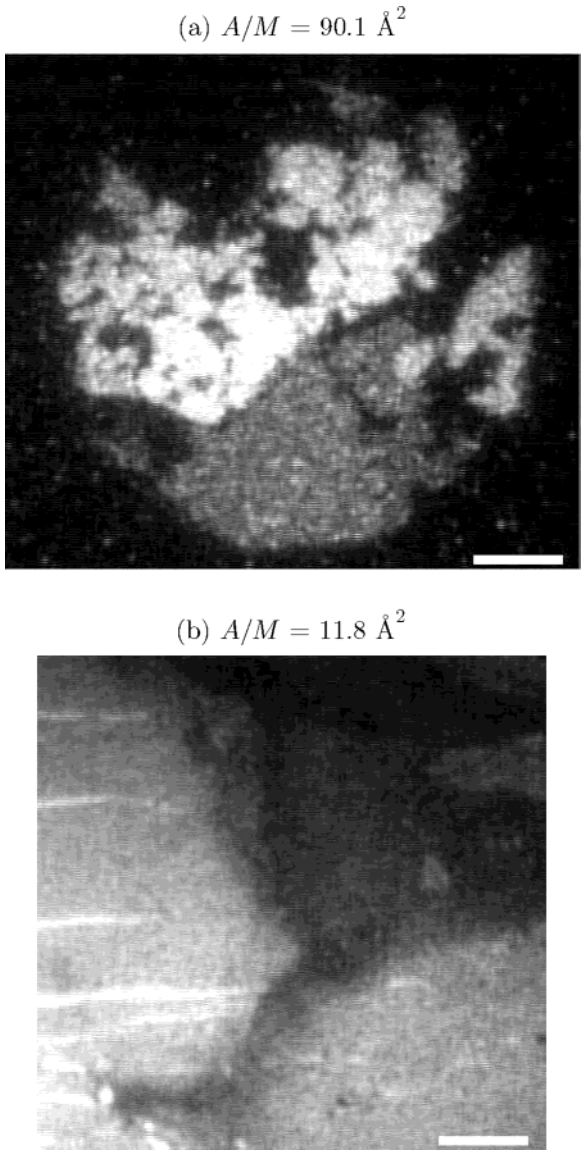

Figure 6. Cholesteryl stearate images under the epifluorescence microscope. (a) Presence of circular and distorted 3D crystalline structures of varying intensity coexisting with voids (gas phase) at very low surface pressure (~0.1 mN/m). (b) Bright streaks over these structures. The scale bar represents 50 μm.

streaks (crystallites) nucleated from the L_2 phase. The BAM image for ChA shows the presence of the L_2 phase with well-defined boundaries coexisting with the G phase even at large *A*/*M* (Figure 7). This texture of L_2 phase indicating a crystalline nature was very different from that seen in the BAM images for the L_2 phase of Ch. Further compression led to the L_2 phase that exhibits a mesh texture. In the collapsed state, bright crystallites were seen to grow from the L_2 phase. These observations were consistent with our epifluorescence studies. The BAM images of ChN are shown in Figure 8. The coexistence of the G and condensed (bright) phase was seen at large *A*/*M* (Figure 8a). We found that the condensed phase was more mobile. Interestingly, we found that the condensed phase melted because of the heat generated by the probe laser of the BAM itself. This led to the growth of G domains. This can be seen even during compression (Figure 8b and c). Further compression led to the formation of a homogeneous condensed phase. In the collapsed state, the condensed phase transformed into brighter dots. These brighter dots coalesced to form circular 3D domains that tended to crystallize with time (Figure 8d).

Figure 7. Brewster-angle microscope image of cholesteryl acetate, showing the coexistence of the G and L_2 phases at $A/M = 186.3$ Å^2. The L_2 phase shows well-defined boundaries. The scale of the image is 6.4×4.8 mm^2.

The BAM images of ChL are shown in Figure 9. At very large *A*/*M*, the G phase coexisted with the condensed phase. With compression, small bright circular condensed domains and still brighter distorted domains were seen to coexist with the G phase (Figure 9a). As in the case of ChN, here also, we found the laser-induced melting of the condensed phase and the growth of the G phase (Figure 9b). At still lower *A*/*M*, more distorted crystalline structures were seen to develop from the condensed phase (Figure 9c). Interestingly, these change in textures were seen at very low surface pressures (0.1 mN/m). For ChM, the BAM image indicated the presence of bright structures even at very large *A*/*M* (Figure 10). The BAM images for ChP showed bright irregular crystalline structure with voids even at very large *A*/*M* (see Supporting Information). Upon compression, the crystalline structure became more dense. BAM images for ChS were similar to those for ChP and showed irregular structures. For ChB, the BAM image (Figure 11) indicated the presence of a crystalline phase with voids (G phase). The crystalline phase appeared bright with irregular boundaries. Upon compression, the voids between regions of this phase were seen to decrease.

For the cholesteryl derivatives, we employed reflection microscopy to probe the textures of the thick 3D domains. Our reflection microscopy studies on ChH and ChO indicated the presence of 3D crystallites immediately after spreading, even at very large *A*/*M*. For the case of ChN, in the collapsed state, we found the presence of circular 3D domains. With time, these domains coalesced to form larger circular 3D domains that were bright in the middle and less bright near the periphery (Figure 12a). These 3D domains, when left overnight, transformed to give a branched (Figure 12b) or dendritic pattern. These patterns were consistent with the textures seen in the epifluorescence and BAM images. The reflection microscope images for ChL were similar to those for ChN. However, the thick domains appeared in the very low surface pressure region (~0.1 mN/m). These thick domains were very fluidlike. They fused into larger domains and tended to crystallize. For ChM, the reflection microscope image (Figure 13) indicated a rigid sheetlike texture with bright branched patterns even at very low surface pressure (~0.1 mN/m). The textures obtained for ChP were very similar to those obtained for ChM. At large *A*/*M*, bright branched patterns were seen over the rigid sheetlike structures. In the case of ChS, very faint circularly shaped 3D domains coexisted with the G phase (Figure 14a). Some of the 3D domains were circular, and others were deformed (Figure 14b). Here, the

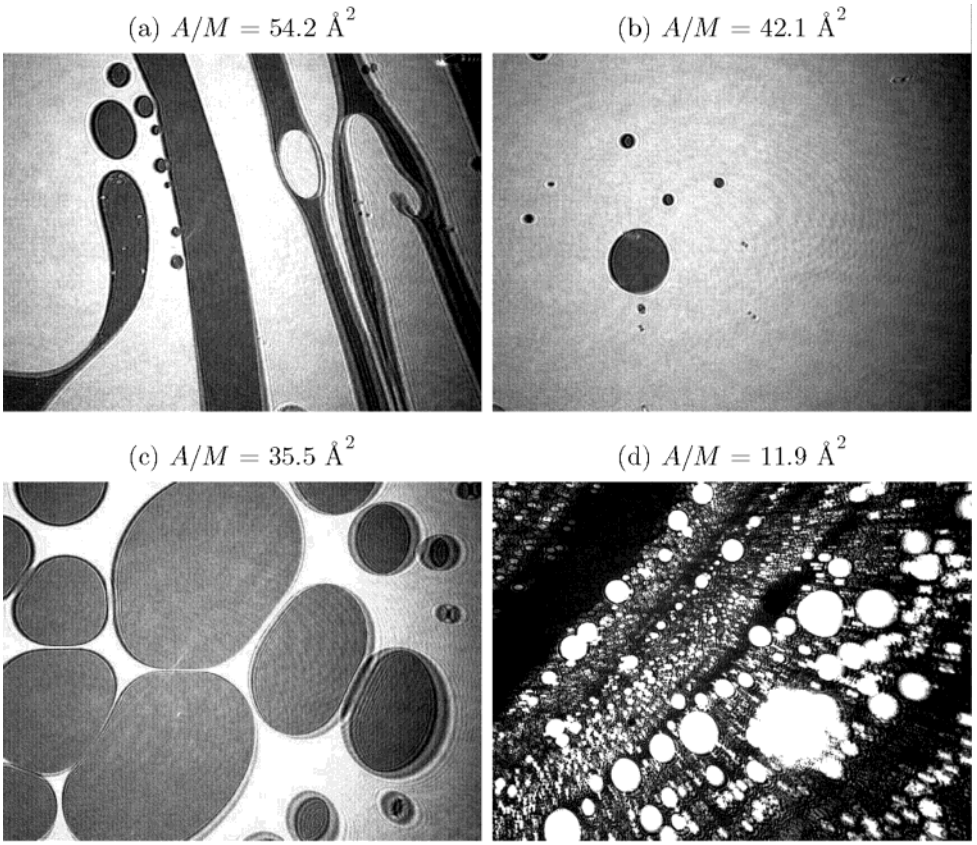

Figure 8. Brewster-angle microscope images of cholesteryl nonanoate. (a) Coexisting gas (dark) and condensed (bright background) phases. (b,c) Growth of the gas domains (dark) due to laser heating. (d) Collapsed state. Here, the brighter dots coalesce to form circular 3D domains that tend to crystallize with time. The scale of each image is 6.4 × 4.8 mm^2.

fluidity of the domains was low, indicating a crystalline nature. In the collapsed state, the 3D domains transformed into distorted patterns.

4. Discussion

For cholesteryl acetate, the $\pi-A/M$ isotherm and the limiting area per molecule, A_0, were almost the same as the corresponding isotherm and A_0 for Ch (~39 Å^2). However, the collapse pressure value for ChA was 16.0 mN/m, which was quite low when compared with the value of 43.0 mN/m for Ch. Interestingly, even though the $\pi-A/M$ isotherm for ChA was similar to that of Ch, the microscope textures were very different. In ChA, under the epifluorescence, the L_2 phase exhibited a mesh texture at large A/M (Figure 2a), whereas for Ch, the L_2 phase appeared homogeneous. This might be due to the presence of the ester group in ChA giving rise to the crystalline nature in the L_2 phase. Grazing-incidence X-ray diffraction (GIXD) studies[4] on ChA also revealed a higher degree of crystallinity in the monolayer phase. The ESP value of 7.1 mN/m reflects the weakly polar nature of the ester group in the ChA molecules. For Ch, an ESP value of 38.1 mN/m shows that the presence of the OH polar group facilitates spreading. This value is in accordance with other reports.[18] Dorfler and Rettig[19] reported $\pi-A/M$ isotherms for the short-chain cholesteryl esters from acetate to butyrate and unstable monolayer behavior for pentanoate. In their case, the decreasing trend in the collapse pressures with increasing alkyl chain length up to butyrate indicated the tendency of the monolayer to become unstable. Cadenhead and Philips[20] reported that cholesteryl butyrate monolayer was unstable and yielded a low collapse pressure of 7 mN/m with an A_0 value of 42 Å^2. Unstable monolayer behavior has also been reported for cholesteryl caproate.[20] For the higher homologues of cholesteryl esters such as ChH and ChO, our studies showed that they formed unstable monolayers. Also, the BAM and reflection microscopy studies indicated the formation of 3D crystallites immediately after spreading. A different behavior was seen for ChN, which is the next higher homologue. On the basis of the A_0 value for ChN, the estimated cross-sectional area of the ChN molecule, and the microscopy observations, we inferred the condensed phase to be a bilayer phase. A similar inference has also been made in the case of cholesteryl myristoleate.[21] The epifluorescence and BAM observations for ChN revealed that this bilayer phase was more fluidlike and coexisted with the G phase (Figures 3a and 8a). In the BAM experiments for ChN, the heat generated by the probe laser melted the bilayer phase, yielding the G phase. Normally, one expects the G phase to decrease in area upon compression. However, in this case, the melting was so dominant that the G phase continued to grow even during compression (Figure 8b and c). In the collapsed state, epifluorescence, BAM, and reflection microscopy studies indicated the existence of 3D domains that were in a metastable state (Figures 3c, 8d, and 12a). Under the reflection microscope, the 3D domains appeared brighter at the center than at the periphery, indicating a nonuniformity in thickness. These domains transformed into crystallites with branched or dendritic patterns. The higher homologue, ChL, yielded a collapse pressure value of 3.0 mN/m and an A_0 value of 16.3 Å^2. The epifluorescence studies indicated the presence of a condensed phase (gray) coexisting with G domains (Figure 4a). These regions transform into bright 3D domains (Figure 4b). The BAM images indicated condensed domains coexisting with the predominantly present G phase. The epifluorescence and BAM textures of the

(a) $A/M = 65.2$ Å^2

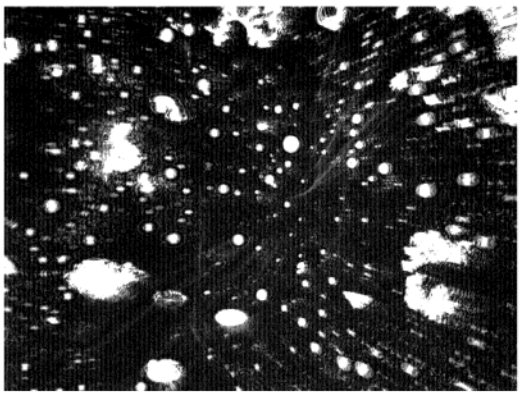

(b) $A/M = 59.8$ Å^2

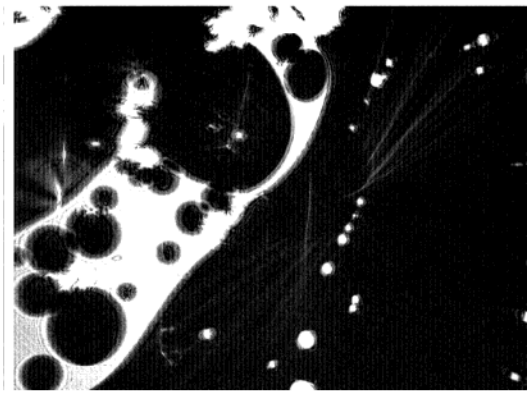

(c) $A/M = 53.7$ Å^2

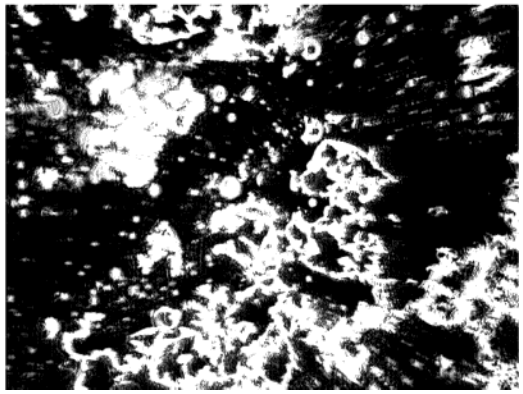

Figure 9. Brewster-angle microscope images of cholesteryl laurate seen at very low surface pressure (~0.1 mN/m). At very large *A*/*M*, coexistence of gas (dark) and condensed (bright) phases was seen. (a) Appearance of still brighter domains that coexist with the condensed domains (bright) and the G phase (dark). The brighter domains were distorted. (b) Melting of the condensed phase and growth of the gas (dark) domains due to laser heating. (c) Transformation of the condensed phase into more distorted crystalline structures. The scale of each image is 6.4 × 4.8 mm^2.

condensed phase of ChL were similar to those of ChN. Here, too, the condensed phase underwent melting due to the probe laser of the BAM. On the basis of these similarities, we suggest that the condensed phase is a bilayer phase. With compression, these bilayer domains transform into 3D domains (Figure 9a and b) and then into crystallites (Figure 9c). This suggestion is also supported by our reflection microscopy studies. These transformations occurred at very low surface pressure (0.1 mN/m), which showed that the ChL bilayer was not stable compared to the bilayer phase of ChN. On the basis of our studies on the ChN and ChL films, we suggest that the homologues that are intermediate between these molecules are likely to yield a bilayer phase at the A−W interface. For cholesteryl tridecanoate, a crystalline bilayer phase has been reported on the basis of surface manometry and GIXD studies.[8] For the higher homologues such as ChM, ChP, and ChS, the isotherms were quite similar, with low A_0 values of about 20 Å^2 and high collapse pressures (~60 mN/m). The A_0 values as compared to the estimated cross-sectional areas of the molecules indicate a bilayer phase in these systems. For ChM and ChP, under epifluorescence, 3D structures were seen with well-defined edges. Dark regions were observed on top of these structures (Figure 5a). Under the reflection microscope, the same dark regions appeared as very bright branched textures (Figure 13). For ChS, under epifluorescence, domains of varying intensity were seen. Under reflection, the ChS films appeared as very faint circular domains. Under BAM, ChM, ChP, and ChS films exhibited irregular crystalline structures at very low surface pressures. In the literature, there are reports stating that ChP and ChS form cloudy, unstable films.[6,7] Recent reports on ChP and ChS suggest the formation of bilayer and thick films according to the results of GIXD and ellipsometry experiments.[8]

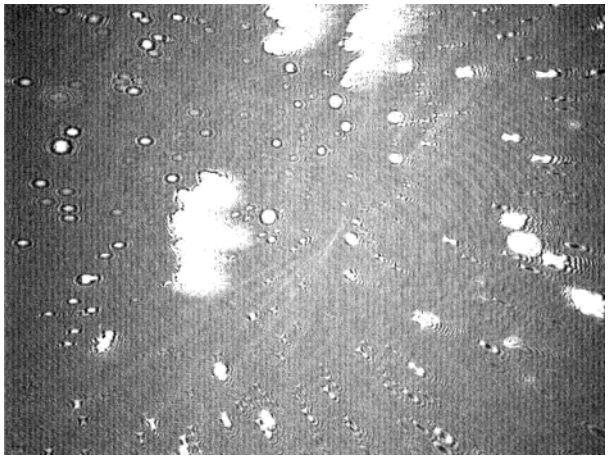

Figure 10. Brewster-angle microscope image of cholesteryl myristate seen at very low surface pressure (~0.1 mN/m), showing the presence of bright irregularly shaped 3D structures coexisting with the gas phase (background) at $A/M = 391$ Å^2. The scale of image is 6.4 × 4.8 mm^2.

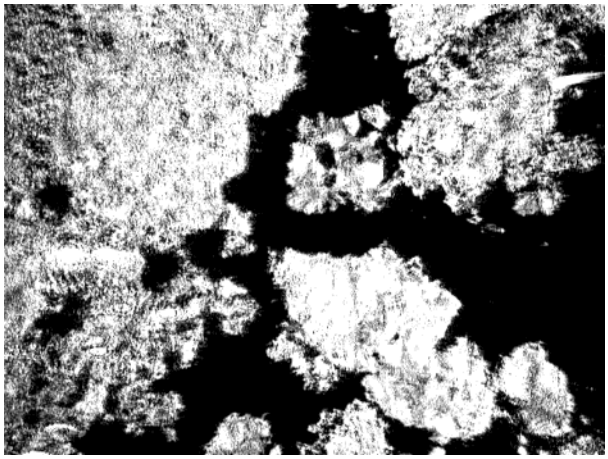

Figure 11. Brewster-angle microscope image of cholesteryl benzoate at very low surface pressure (~0.1 mN/m), showing the domains having irregular boundaries (crystalline) with voids (gas phase) at $A/M = 46.8$ Å^2. The scale of each image is 6.4 × 4.8 mm^2.

(a) $A/M = 11.0$ Å^2

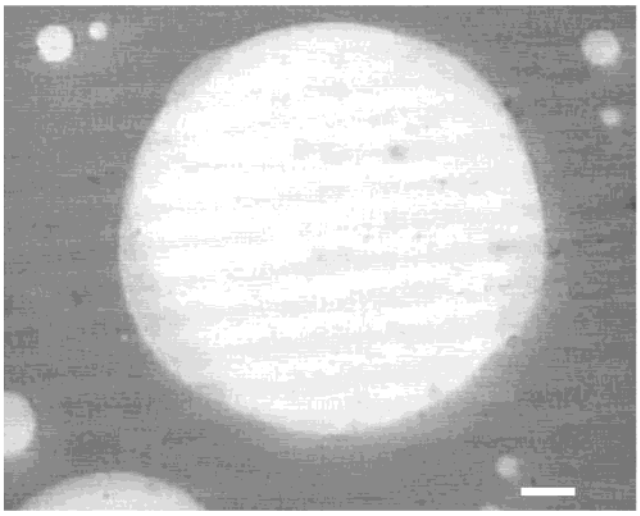

(b) $A/M = 11.0$ Å^2

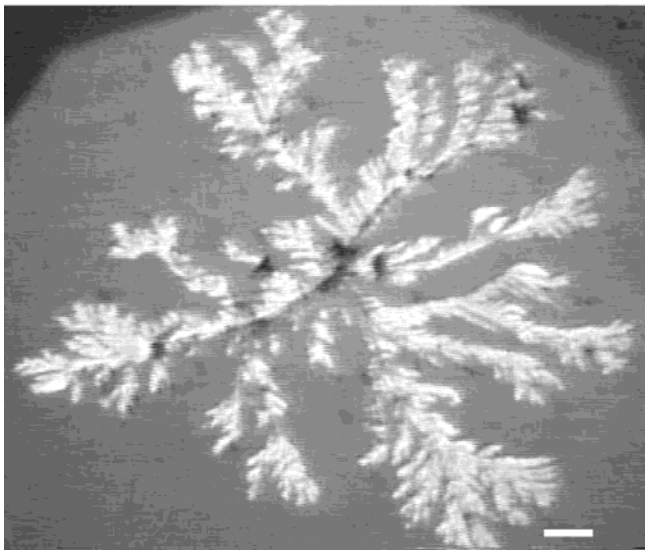

Figure 12. Reflection microscope images of cholesteryl nonanoate in the collapsed state. (a) Collapsed state with metastable bright circular 3D domains. Here, the bright 3D domains coalesced with time to yield larger domains. These larger domains were more intense at the center and appeared weaker toward the periphery. (b) Evolution of a bright circular 3D domain into a branching pattern. The scale bar represents 10 μm.

On the basis of our $\pi-A/M$ isotherms and microscopy observations on ChM, ChP, and ChS esters, we inferred that they exhibited a coexistence of crystalline bilayer and 3D structures at very low surface pressures.

According to Craven,[12] the packing of cholesteryl derivatives in the bulk has been classified broadly into three types (Figure 15) according to the interactions between the different parts of the molecules, namely, cholesteryl−cholesteryl (m-i), cholesteryl−chain (m-ii), and chain−chain (bilayer) interactions. The short-chain cholesteryl esters from cholesteryl caproate to cholesteryl octanoate have been classified as type m-i. The other intermediate esters from cholesteryl nonanoate to cholesteryl laurate were classified as type m-ii. Still higher homologues of cholesteryl esters from cholesteryl tridecanoate onward were classified as bilayer-type packing. For the case of unsaturated esters of cholesterol, both m-i- and m-ii-type packing have been

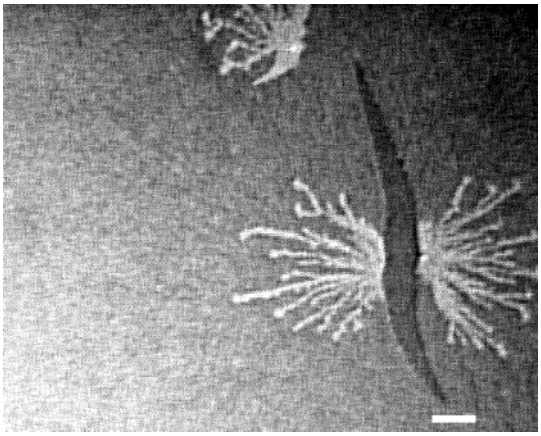

Figure 13. Image of cholesteryl myristate under the reflection microscope at very low surface pressure (~0.1 mN/m), showing the presence of fractures between the rigid sheets and the growth of very bright branched crystallites over the sheets at $A/M = 97.0$ Å^2. The scale bar represents 10 μm.

(a) $A/M = 91.6$ Å^2

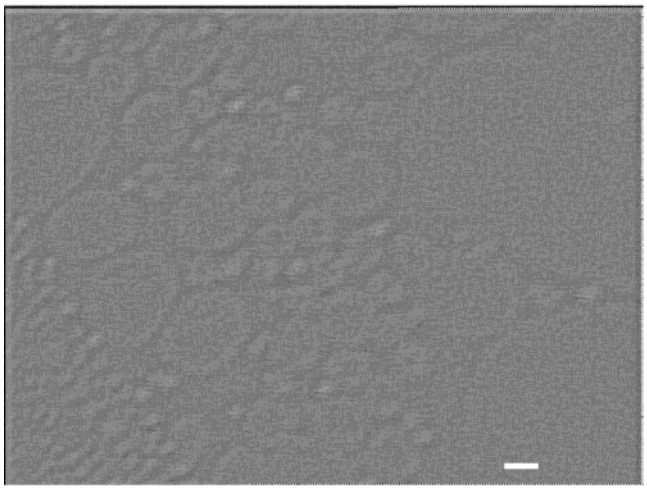

(b) $A/M = 59.7$ Å^2

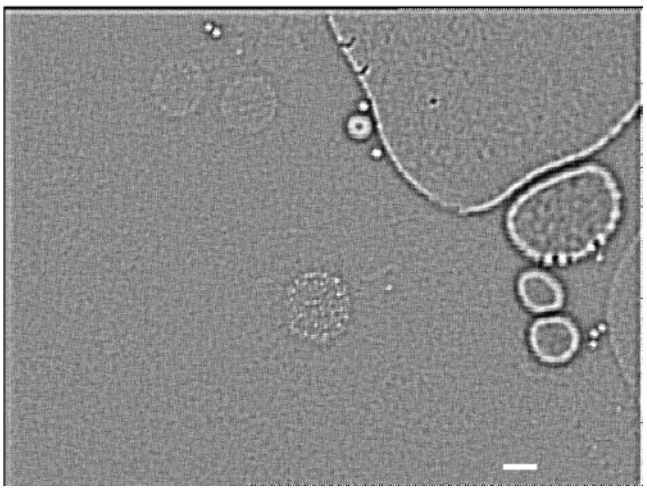

Figure 14. Images of cholesteryl stearate under the reflection microscope at very low surface pressure (~0.1 mN/m). (a) Presence of very faint circular 3D domains. (b) 3D domains that become deformed and coalesce into larger domains. The scale bar represents 10 μm.

reported. On the basis of our studies on the cholesteryl derivatives, we suggest a correlation between the packing of

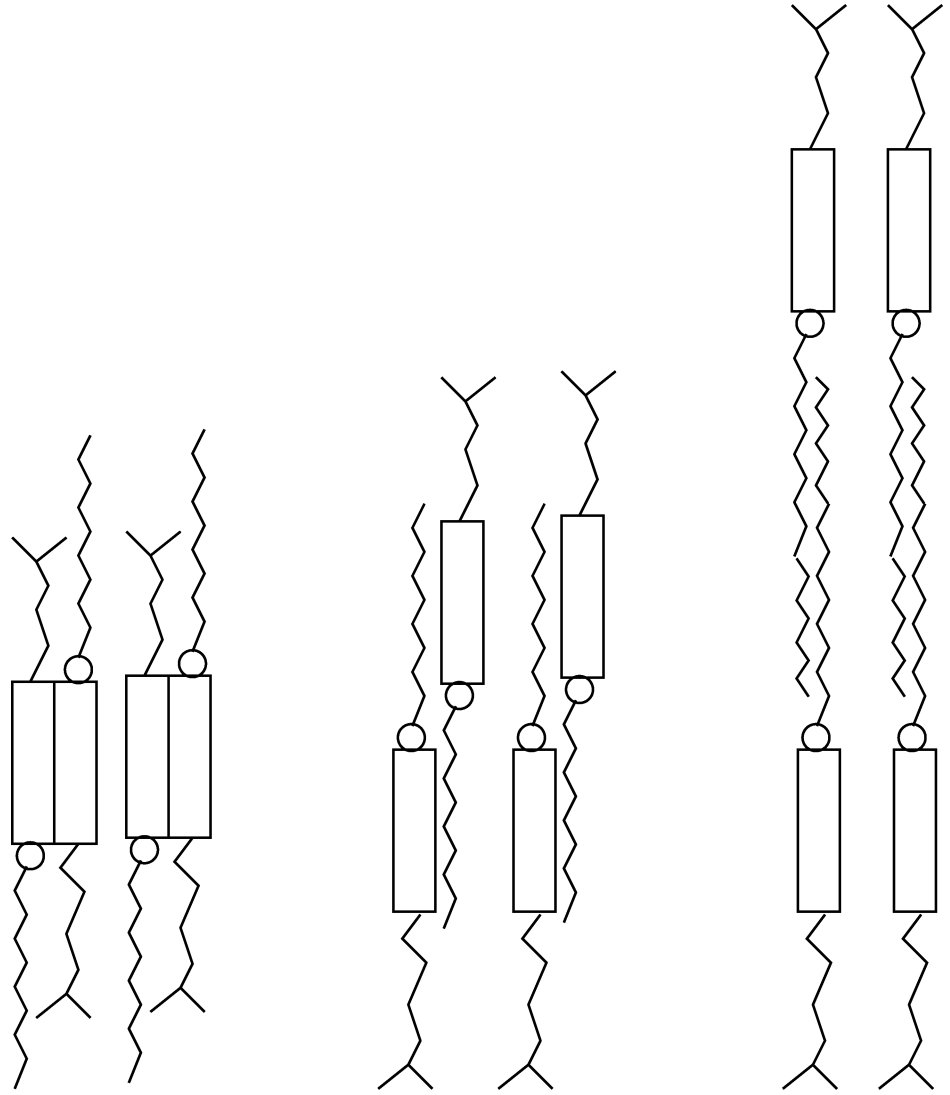

Figure 15. Schematic representations of different packings for cholesteryl esters in the bulk. (a) m-i packing of the cholesteryl esters from cholesteryl caproate to cholesteryl octanoate. (b) m-ii packing of the cholesteryl esters from cholesteryl nonanoate to cholesteryl laurate. (c) Bilayer packing of higher homologues of the cholesteryl esters from cholesteryl tridecanoate onward.

the molecules in the bulk and the packing in the different phases at the A−W interface for some members. The esters such as ChH and ChO that are characterized by m-i-type packing yielded 3D crystallites immediately upon spreading at the A−W interface. Cholesteryl nonanoate, which comes under the classification of m-ii packing, yielded a bilayer phase (fluidlike) at the A−W interface. ChL, which exhibits m-ii packing, also yielded a bilayer phase but tended to crystallize at very low surface pressure. The higher homologues such as ChM, ChP, and ChS, which come under the classification of bilayer packing, showed coexisting gas, bilayer (crystalline), and 3D structures at the A−W interface.

The $\pi-A/M$ isotherm for ChOl (see Supporting Information) indicated that the monolayer had a collapse pressure of 8.2 mN/m and an A_0 value of 114.3 Å^2. To account for this high value of A_0, Smaby and Brockman[22] proposed that the ester group is inside the subphase and the cholesteryl moiety and alkyl chains are lifted up in the air. Our microscopy studies showed the phase sequence for ChOl to be coexisting G and L_1 phases,[23] followed by the L_1 phase, and then coexisting L_1 phase and multilayers. The $\pi-A/M$ isotherm for ChOC (see Supporting Information) yielded a collapse pressure of 3.4 mN/m and an A_0 value of 28.7 Å^2. Our microscopy observations indicated the phase sequence to be coexisting G phase, L_1' phase,[24] and traces of L_1 phase; coexisting L_1 and L_1' phases; and coexisting L_1' phase, multilayers, and bright domains (see Supporting Information).

In the case of ChB, we found a high collapse pressure of about 60 mN/m and an A_0 value of 23.7 Å^2. The A_0 value corresponds to one-half of the cross-sectional area of ChB molecules, suggesting bilayer formation at the A−W interface. We found a drop in the surface pressure when compression was stopped at a given A/M value in the steep region of the $\pi-A/M$ isotherm. BAM studies showed textures with irregular, sharp boundaries and voids (Figure 11). From these observations, we inferred that ChB forms a crystalline bilayer phase. Under the reflection microscope, the nucleation of 3D crystallites from the homogeneous crystalline bilayer phase could be observed at high surface pressures. The unstable nature of the crystalline bilayer phase seen in the steep region of the isotherm (when compression was stopped) can be attributed to the formation of 3D crystallites. These observations contradict an earlier publication on ChB that reported the formation of a stable monolayer[25]

TABLE 1: Phases of Cholesteryl Derivatives at the Air−Water Interface

materials	π_c (mN/m)	A_0 (Å^2)	phases at the A−W interface
Ch	43.0	38.8	G + L_2, L_2, L_2 + 3D crystallites
ChA	16.0	38.9	G + L_2, L_2 (crystalline in nature), L_2 + 3D crystallites
ChH, ChO	−	−	no monolayer formation (3D crystallites)
ChN	2.5	22.0	G + bilayer (fluidlike), bilayer, bilayer + metastable 3D domains (transforms to 3D crystallites)
ChL	3.0	16.3	G + bilayer (fluidlike) + 3D crystallites
ChM, ChP, ChS	∼60	19.6, 20.7, 21.4	G + bilayer (crystalline) + 3D structures
ChB	∼60	23.7	G + bilayer (crystalline), 3D crystallites

and that also reported a very high value of A_0 that is twice the value indicated by our $\pi-A/M$ isotherm.

There are some studies reporting the coexistence of G and bilayer phases.[8,26,27] Bilayer formation due to the interdigitation of alkyl chains has been found in molecules with large differences in the cross-sectional areas of their hydrophobic parts.[8,27] Weinbach et al.[28] reported that hydrophobic materials such as alkanes can give rise to the coexistence of crystalline monolayers and multilayers or coexisting thin crystallites and multilayers depending on chain length. Our results on ChN and ChL indicated the spontaneous formation of a fluidlike bilayer. The fluidity of the bilayer phase can be attributed to the interaction between the cholesterol skeleton and the alkyl chain. This is different from the cholesteryl−cholesteryl and chain−chain interactions that lead to crystalline structures. The various phases of the cholesteryl derivatives at the A−W interface are summarized in Table 1.

The assembly of molecules at the A−W interface can also be related to the liquid-crystalline phases of the cholesteryl esters in the bulk. The homologues from ChA to ChO exhibit a cholesteric phase, whereas the homologues from ChN onward exhibit a smectic phase in addition to the cholesteric phase.[12] Thus, the formation of a bilayer by ChN might be related to the onset of the smectic phase. It will be interesting to connect these properties with the role played by cholesteryl esters inside a lipoprotein. On the basis of X-ray and other studies on low-density lipoproteins (LDLs), a suggestion has been made that the shape changes of LDLs be associated with the transition from the smectic phase to a disordered phase in cholesteryl esters.[1] Hence, it would be interesting to undertake further studies on the cholesteryl derivatives and their mixtures to relate their assembly at the A−W interface, their mesogenic behavior, and their role in lipoproteins.

5. Conclusions

Although surface manometry studies have been carried out on some of the cholesteryl derivatives, there has not been a detailed microscopy studies on them. Here, we report a detailed study on the phases, molecular aggregation, and structures of cholesteryl derivatives at the air−water interface employing surface manometry, epifluorescence, BAM, and reflection microscopy. The short-chain cholesteryl ester cholesteryl acetate forms a stable monolayer with a relatively low collapse pressure when compared to cholesterol. The homologues such as cholesteryl heptanoate and cholesteryl octanoate tend to form 3D crystallites. Interestingly, for cholesteryl nonanoate, we found a fluidlike bilayer phase at the air−water interface. The higher homologue cholesteryl laurate exhibits bilayer formation at very large A/M, but it has a tendency to crystallize when compared to cholesteryl nonanoate, even at very low surface pressures. We suggest that the bilayer phases can also occur at the A−W interface even for homologues such as cholesteryl decanoate and undecanoate that are between cholesteryl nonanoate and cholesteryl laurate. For cholesteryl myristate, cholesteryl palmitate, and cholesteryl stearate, our $\pi-A/M$ studies indicated the formation of a bilayer (crystalline) phase. The microscope studies indicated the unstable nature of the bilayer phase that coexists with 3D structures. Cholesteryl benzoate forms a crystalline bilayer phase. We can broadly associate the assembly of molecules in different phases at the A−W interface with the packing of the cholesteryl esters in the bulk.

Supporting Information Available: Surface pressure−area per molecule isotherms of ChOC and ChOl. Epifluorescence image of ChM. Brewster-angle microscope images of ChP. Epifluorescence images of ChOC. This material is available free of charge via the Internet at http://pubs.acs.org.

References and Notes

(1) Segrest, J. P.; Jones, M. K.; Loof, H. D.; Dashti, N. *J. Lipid Res.* **2001**, *42*, 1346.
(2) Lundberg, B. *Chem. Phys. Lipids* **1975**, *14*, 309.
(3) Simons, K.; Ikonen, E. *Science* **2001**, *290*, 1721.
(4) Rapaport, H.; Kuzmenko, I.; Lafont, S.; Kjaer, K.; Howes, P. B.; Als-Nielsen, J.; Lahav, M.; Leiserowitz, L. *Biophys. J.* **2001**, *81*, 2729.
(5) Lafont, S.; Rapaport, H.; Somjen, G. J.; Renault, A.; Howes, P. B.; Kjaer, K.; Als-Nielsen, J.; Leiserowitz, L.; Lahav, M. *J. Phys. Chem. B* **1998**, *102*, 761.
(6) Adam, N. K.; Jessop, G. *Proc. R. Soc. London, Ser. A* **1928**, *120*, 473.
(7) Kwong, C. N.; Heikkila, R. E.; Cornwell, D. G. *J. Lipid Res.* **1978**, *12*, 31.
(8) Alonso, C.; Kuzmenko, I.; Jensen, T. R.; Kjaer, K.; Lahav, M.; Leiserowitz, L. *J. Phys. Chem. B* **2001**, *105*, 8563.
(9) von Tscharner, V.; McConnel, H. M. *Biophys. J.* **1981**, *36*, 409.
(10) Knobler, C. M. *Science* **1990**, *249*, 870.
(11) Honig, D.; Mobius, D. *J. Phys. Chem.* **1991**, *95*, 4590.
(12) Small, D. M.; Ed. *The Physical Chemistry of Lipids. Handbook of Lipid Research*; Plenum Press: New York, 1986; Vol. 4.
(13) Ybert, C.; Lu, W.; Moller, G.; Knobler, C. M. *J. Phys. Chem. B* **2002**, *106*, 2004.
(14) Suresh, K. A.; Bhattacharyya, A. *Langmuir* **1997**, *13*, 1377.
(15) Slotte, J. P.; Mattjus, P. *Biochim. Biophys. Acta* **1995**, *22*, 1254.
(16) We represent the condensed phase as the L_2 phase, where the monolayer was less mobile and appeared less bright under the epifluorescence microscope. In the literature, this phase is also referred to as the liquid condensed phase.
(17) Seoane, R.; Minones, J.; Conde, O.; Minones, J., Jr.; Casas, M.; Iribarnegaray, E. *J. Phys. Chem. B* **2000**, *104*, 7735.
(18) Iwahashi, M.; Iwafuji, A.; Minami, H.; Katayama, N.; Iimura, K.; Kato, T. *Mol. Cryst. Liq. Cryst.* **1999**, *337*, 117.
(19) Dorfler, H. D.; Rettig, W. *Colloid Polym. Sci.* **1982**, *260*, 802.
(20) Cadenhead, D. A.; Philips, M. C. *J. Colloid Interface Sci.* **1967**, *24*, 491.
(21) Smaby, J. M.; Brockman, H. L. *Biochemistry* **1981**, *20*, 718.
(22) Smaby, J. M.; Brockman, H. L. *Biochemistry* **1984**, *23*, 3312.
(23) We represent the low-density phase as the L_1 phase, where the monolayer was more mobile and bright under the epifluorescence microscope. In the literature, this phase is also referred to as the liquid expanded phase.
(24) The L_1' phase appeared to be a variant of the L_1 phase and was comparatively less bright.
(25) Mukherjee, S.; Chatterjee, R.; Bose, S. K. *Chem. Phys. Lipids* **1978**, *23*, 85.
(26) Gershfeld, N. L.; Tajima, K. *Nature* **1979**, *279*, 708.
(27) El Abed, A.; Pouzet, E.; Faure, M.-C.; Saniere, M. *Phys. Rev. E* **2000**, *62*, R5895.
(28) Weinbach, S. P.; Weissbuch, I.; Kjaer, K.; Bouwman, W. G.; Als-Nielsen, J.; Lahav, M.; Leiserowitz, L. *Adv. Mater.* **1995**, *7*, 857.